BIOCHEMISTRY
including biophysical chemistry & molecular biology

Article

pubs.acs.org/biochemistry

Combined Density Functional Theory (DFT) and Continuum Calculations of pK_a in Carbonic Anhydrase

Dian Jiao and Susan B. Rempe*

Center for Biological and Materials Sciences, MS 0895, Sandia National Laboratories, Albuquerque, New Mexico 87185, United States

ABSTRACT: Deprotonation of zinc-bound water in carbonic anhydrase II is the rate-limiting step in the catalysis of carbon dioxide between gas- and water-soluble forms. To understand the factors determining the extent of dissociation, or pK_a, of the zinc-bound water, we apply quantum chemistry calculations to the active site coupled with a continuum model of the surrounding environment. Experimentally determined changes in pK_a associated with mutations of the active site are well reproduced by this approach. Analysis of the active site structure and charge/dipole values provides evidence that mutations cause changes in both conformation of the active site structure and local polarization, which accounts for the shifts in pK_a. More specifically, the shifts in pK_a correlate with the dipole moments of the zinc-bound water upon deprotonation. The data further support the conclusion that the distinct pK_a values found in mutations of the same type, but applied to different sites, result from asymmetric ligation and different electronic environments around the zinc ion.

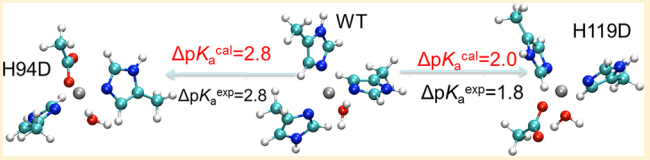

Developing efficient techniques for carbon dioxide (CO_2) sequestration remains a priority because of the continuously increasing atmospheric level of CO_2, which is the main cause of global warming.[1] About 80% of the annually added CO_2 is removed from the air through either dissolution in the oceans or absorption by living organisms. Dissolution proceeds slowly, first with solvation of the neutral gas by water, followed by hydration reactions that convert carbon dioxide to water-soluble forms such as bicarbonate ion (HCO_3). In plants and animals, carbonic anhydrase enzymes facilitate CO_2 absorption by catalyzing the interconversion of carbon dioxide and bicarbonate ion via hydration and dehydration reactions. Carbonic anhydrase is one of the fastest enzymes of all, with forward and reverse reaction rates on the order of 10^6 s^{-1}.[2,3] Therefore, understanding the mechanisms of CO_2 hydration by liquid water and CO_2−bicarbonate conversion by carbonic anhydrase enzymes can lay the groundwork to help design artificial programmable biopolymers to sequester, and release, CO_2 efficiently. In a prior work, we studied the hydration of neutral CO_2 in water with quasi-chemical theory.[4] In this study, we focus on the enzyme.

Type II carbonic anhydrase (CA II), which exists in the human body, assists in the separation, uptake, and transport of CO_2 in the lungs and circulatory systems. CA II catalyzes the reversible hydration of carbon dioxide at its zinc-centered active site. The zinc ion (Zn^{2+}) is coordinated with three histidine residues (H94, H96, H119) plus a water molecule (H_2O) arranged in a tetrahedral geometry, according to crystal structure data of the CA II active site (PDB ID 2CBA).[5]

Figure 1 illustrates the widely accepted model of the carbonic anhydrase catalytic conversion of carbon dioxide to bicarbonate ion, which is based on a large number of experimental[6−11] and theoretical investigations.[12−22] In the first step of the catalytic cycle, the zinc-bound water forms zinc-bound hydroxide ion after losing a proton (H^+) through a proton-transfer process. In the second step, a CO_2 molecule enters the catalytic site and forms a bicarbonate ion by reacting with the deprotonated water, OH^-, which is still bound to zinc. The zinc-bound bicarbonate ion undergoes intramolecular structural rearrangement before it is replaced by a nearby water molecule in the final step, by which the active site recovers its original form.[23]

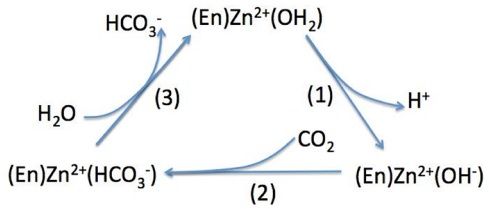

Figure 1. Key reactions in the reversible conversion of CO_2 to bicarbonate ion by carbonic anhydrase (represented by *En*).

Much of the prior work in the literature has focused on the proton transfer mechanism associated with the first step of the catalytic cycle in Figure 1. In this ongoing debate, some advocate transport of the dissociated water proton out of the active site by "proton hops"[24,25] while others advocate a "proton holes" mechanism.[26,27] The nature of the water bridge involved in the proton relay, especially the number of water molecules, is similarly debated.[28] Nevertheless, there is a general consensus that deprotonation of the zinc-bound water is the rate-limiting step in the catalytic reaction. Further, deprotonation triggers the whole process. Therefore understanding the factors that determine the acidity of the zinc-

Received: November 30, 2011
Revised: June 22, 2012
Published: June 25, 2012

   dx.doi.org/10.1021/bi201771q | *Biochemistry* 2012, 51, 5979−5989

bound water, characterized by the equilibrium acid dissociation constant (K_a), or its logarithm (pK_a), is important for understanding the catalytic mechanism of carbonic anhydrase.

The pK_a of the zinc-bound water in the wild type carbonic anhydrase II is 6.8.[29] For comparison, the pK_a value of a water molecule in bulk conditions is 15.7,[30] substantially higher than water at the active site of CA II. A smaller pK_a value indicates that water in the active site of CA II is more acidic and thus deprotonated to a greater extent than bulk water. A single mutation of one of the zinc-coordinating ligands dramatically increases the pK_a of the zinc-bound water. In particular, replacing a single histidine (H or Hist) with aspartic acid (D or Asp), such as H119D or H94D, results in a shift in pK_a of the zinc-bound water to 8.6 and 9.6, respectively.[29] This phenomenon implies that replacing a histidine ligand with a negatively charged aspartate stabilizes water relative to its dissociated form, thus significantly hindering loss of a proton from the zinc-bound water. Since catalysis initiates with deprotonation of the zinc-bound water, understanding the factors that determine pK_a of the water will aid in understanding the mechanism of the catalytic activity of carbonic anhydrase.

In this work, we investigate the pK_a shifts of zinc-bound water due to mutations to the active site of CA II using a density functional theory (DFT)/continuum technique. Our calculations and analyses support the conclusion that changes in conformation and electronic polarization in mutated active sites account for altered deprotonation behavior of the zinc-bound water. These insights into the origin of the catalytic reaction of the enzyme should help design artificial materials that mimic the function of the carbonic anhydrase enzyme to capture CO_2 efficiently.

pK_A PREDICTIONS

In general, the logarithm of the acid dissociation constant for a molecule, pK_a, can be estimated by calculating the free energy of deprotonation, scaled by absolute temperature (T) and the gas constant (R), based on the following relationship:[31]

$$pK_a = \frac{\Delta G_{env}^{deprot}}{RT \ln 10} \quad (1)$$

The free energy of deprotonation, ΔG_{env}^{deprot}, is the change in free energy for losing a proton to the surrounding environment, here defined by solvent and protein.

The free energy change is commonly estimated by free energy perturbation (FEP) with atomistic simulations,[32] first introduced and applied to pK_a calculations on protein residues by Warshel et al. in 1986.[33] A number of studies used the empirical valence bond method[16,17,34] to estimate the catalytic reaction energies and pK_a's in enzymes, including carbonic anhydrase. A simpler method, the linear response approximation (LRA) in combination with a protein dipole/Langevin dipoles (PDLD) model, also can predict pK_a with reasonable accuracy.[35] Attempts have been made to evaluate pK_a in proteins using molecular mechanics and generalized Born surface area (MM-GBSA) methods based on molecular dynamics simulation trajectories coupled to implicit solvation models.[36−38] Predictions of pK_a from molecular mechanics approaches sometimes deviate significantly from experimental values.[39] Moreover, these predictions are based on assumptions about the protonation states of the protein residues and the known pK_a values of the amino acids in bulk.[38,39]

Quantum mechanical (QM) methods provide more reliable predictions of pK_a. The first successful applications, by the Karplus group in the early 90s, predicted pK_a values for small molecules in solution using quantum mechanics to describe the molecule and continuum models to describe the surrounding solvation environment.[31,40] In recent years, pK_a predictions for small molecules have used quantum mechanics based on DFT, coupled with a polarizable continuum model (PCM) of the solvation environment.[41,42] A more rigorous ab initio molecular dynamics (AIMD) simulation technique used by Leung, et al. correctly predicted the pK_a of ionic groups at the surface of silica.[43]

Because of the computational demand, it is impractical to treat a whole protein with QM to calculate pK_a values. Alternatively, a hybrid quantum mechanical/molecular mechanical (QM/MM) potential can be used to estimate pK_a values in macromolecules. Cui's group carried out extensive pK_a calculations on various proteins with quantitative accuracy.[44−49] Kamerlin et al. reported an accelerated QM/MM scheme to calculate the pK_a in enzymes and obtained properly converged results.[50]

In this study, we apply DFT to the zinc-centered active site of carbonic anhydrase II, coupled to an implicit model of the surrounding environment, to estimate changes in pK_a of the zinc-bound water with mutations. Bottoni[51] and Miscione[52] applied a similar macroscopic solvation model to study other aspects of the catalytic mechanism of carbonic anhydrase. Their calculations helpfully interpreted the experimental data on proton transfer reaction rates.

In our work, the DFT-continuum approach follows the formulation of quasi-chemical theory (QCT), a rigorous statistical mechanical framework for free energy calculations in which free energy is divided into local and distant solvent contributions.[53,54] Here we choose the active site, composed of the zinc ion and its ligating residues, as the local solvation environment for the proton. We treat the active site quantum mechanically to capture the highly polar local environment around zinc. A dielectric continuum represents the distant solvation environment. This representation assumes that the environment influences the active site mainly through long-ranged dispersive and electrostatic interactions. The environment may also influence the structure of the active site.[55−57] Since our studies pertain to mutations applied only to the active site, we assume that the environment permits rearrangements of the active site to lowest energy structures.[58] The energy-minimized structure of the wild type carbonic anhydrase active site supports this assumption as it deviates only modestly from the crystal structure (see below). Finally, we focus on the relative pK_a changes caused by active-site mutation, rather than absolute pK_a values. Thus, the long-ranged interactions from the protein environment do not play as critical a role on water deprotonation as the local chemistry at the active site. Therefore, we argue that the QM/continuum method applies in this case.

The theory and methodology of QCT, both in its original form as a liquid state theory and in its adaptation to heterogeneous environments like proteins, have been discussed in detail previously.[57−59] Furthermore, an explicit test confirmed the equivalence of QCT, based on a DFT minimum energy description of ions and their ligating waters coupled to a dielectric continuum model of the remaining environment, with thermodynamic integration using a full ab initio molecular dynamics simulation.[60] In prior work, QCT applied to ions

dx.doi.org/10.1021/bi201771q | Biochemistry 2012, 51, 5979−5989

predicted hydration properties of monovalent[61−65] and divalent ions[66,67] as well as the hydration properties of nonpolar molecules.[4,68−72] Moreover, QCT with a QM/continuum approach has proven to be a consistent approach for modeling metal binding site in proteins as well. For example, QCT was employed to examine K^+/Na^+ selectivity in potassium channel proteins by studying the relationship between constraints on binding site composition and configuration and free energies for selective ion binding from water.[55−57,73] A QCT thermodynamic cycle that incorporated these structural constraints was recently formulated for calculating solvation free energies of ions in proteins by applying coordination constraints at the ion binding site.[58]

COMPUTATIONAL METHODS

The pK_a shifts due to the His/Asp mutations at the active site of CA II are estimated as the differences in pK_a for wild type and mutant enzymes. The shift in pK_a can be translated from the difference in deprotonation free energies of wild type (WT) and mutant (MT) proteins via eq 1. The deprotonation free energies can be computed from standard thermodynamic cycles (see, for example, ref 74) shown in Scheme 1. Reference 75 defines the relationship between this cycle and quasi-chemical theory.

Scheme 1

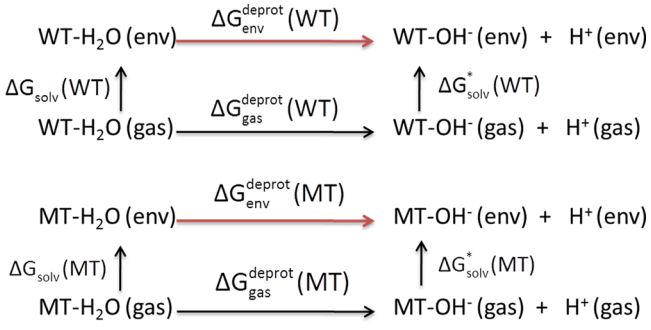

$$\Delta G_{env}^{deprot}(X) = \Delta G_{gas}^{deprot}(X) + \Delta G_{solv}^{*}(X) + \Delta G_{solv}^{H^+} - \Delta G_{solv}(X) \quad (2)$$

$$X = \text{WT or MT}$$

Direct calculation of deprotonation free energy in the environment surrounding the active sites (red arrows in the thermodynamic cycles) is somewhat complicated because the proton must be turned off gradually in multiple steps during free energy perturbation analysis. Alternatively, we can follow the other path in the cycle to calculate the deprotonation free energy in a more convenient way.

According to eq 2, the deprotonation free energy in the environment (ΔG_{env}^{deprot}) is the sum of the deprotonation free energy in the gas phase (ΔG_{gas}^{deprot}) and the solvation free energy contributions (ΔG_{solv}) from products (X−OH$^-$, symbolized by *, and H$^+$) and reactant (X−H_2O) in the deprotonation reaction. In this calculation, we only take into account two discrete end-point states in the gas phase, which are the protonated (X−H_2O) and deprotonated (X−OH$^-$) active sites. Thus, ΔG_{gas}^{deprot} is given by the difference in free energies for active-site product and reactant ($G_{gas}^{*} - G_{gas}$). Since we ultimately seek the relative deprotonation free energy between mutant (MT) and wild type (WT) enzymes, $\Delta\Delta G_{env}^{deprot} = \Delta G_{env}^{deprot}$ (MT) − ΔG_{env}^{deprot} (WT) or the related ΔpK_a (see eq 1), the solvation free energy of the proton in bulk liquid water (ΔG_{solv}^{H+} ranging from −265 to −251 kcal/mol), which is challenging to compute,[42,76] cancels out. Thus, we include only contributions from the active site in the total solvation free energy calculated for a single deprotonation reaction, $\Delta\Delta G_{solv} = \Delta G_{solv}^{*} - \Delta G_{solv}$.

The starting structure of the wild type enzyme is taken from the X-ray crystal structure of human carbonic anhydrase II determined by Hakansson et al. at 1.54 Å resolution (PDB ID 2CBA).[5] In the wild type enzyme, the active site consists of a zinc ion (Zn 262), three histidine residues (His 94, His 96, and His 119), and a water molecule (H_2O 263). Only the active site structure is under explicit consideration in gas phase calculations due to the following reasons. First, deprotonation occurs at the active site of the enzyme. Although the rest of the protein also affects the pK_a of the zinc-bound water, we assume that details of the surroundings are not as crucial as for these polar residues directly coordinating with zinc. Thus the surrounding protein and solution environment will be represented with a coarser continuum method that accounts for electrostatic and long-ranged dispersive interactions with the active site, as discussed below.

Second, we are computing the pK_a change (ΔpK_a) between wild type and mutant enzymes. The mutations also occur at the active site. For both wild type and mutant enzymes, we assume the environment permits structural rearrangements of the active site to achieve low energy conformations. This proposition is supported by the observation that the predicted lowest energy active site structure of the wild type enzyme closely matches the crystal structure (as described below).

Lastly, DFT calculations are computationally demanding. Taking into account more atoms requires more computational resources, but is not necessarily needed. Prior tests of ion solvation in water in fact confirmed that local application of QM coupled to continuum descriptions of the environment can be sufficient. Specifically, free energy calculations based on a minimum energy QM description of an ion and its coordinating ligands, coupled to a continuum model of the remaining environment, gave nearly identical hydration free energies as when based on a full ab initio molecular dynamics simulation.[60] Comparison of predicted shifts in pK_a values between wild type and mutants with those measured by experiment help confirm that these approximations are valid.

The active-site cluster is further simplified by truncating the backbones of the histidines; hence, three ligands of zinc in the active site become imidazole molecules. In the mutant clusters, we replace one histidine with a negatively charged aspartic acid molecule truncated to acetate anion. Truncation of the histidine backbones is also performed in the mutant structures. The PYMOL program[77] is used to determine initial positions for hydrogen atoms and the mutated residues based on the wild type crystal structure.

A total of four types of inner-shell clusters representing various active sites are constructed for the studies: wild type (WT) protonated; wild type (WT) deprotonated; mutated (MT) protonated; mutated (MT) deprotonated. To calculate deprotonation free energy in the gas phase (ΔG_{gas}^{deprot}), each cluster is first energy-minimized with the hybrid B3LYP density functional and the 6-311+G(2d,p) basis set using the Gaussian 09 quantum chemistry package.[78] The choice of B3LYP/6-311+G(2d,p) level of theory is based on its overall balance of computational efficiency and accuracy.[4,66] Single point energies for the lowest energy structures are calculated in the same way.

dx.doi.org/10.1021/bi201771q | Biochemistry 2012, 51, 5979−5989

Vibrational frequencies are evaluated to ensure that no significant imaginary components exist, thus confirming that the geometries are fully minimized in potential energy. The frequency calculations also yield estimates of zero-point energy (ZPE) and thermal corrections to the electronic energy estimated at room temperature and standard pressure, 298.15 K and 1 atm.

The solvation free energies (ΔG_{solv}) are computed with the APBS package[79] by treating the system beyond the active site clusters as a dielectric continuum. The calculation is done at room temperature, 298.15 K. A dielectric constant of $\varepsilon = 1$ is used for the solute, or active site cluster. To describe the environment, we use $\varepsilon = 40.0$ to represent the collective electrostatic contributions from both the surrounding protein and solvent. According to Warshel et al., a continuum model with dielectric constant value 40 is optimal to describe the charge−charge interactions in proteins.[80] By using a similar dielectric constant, success has been achieved by Miscione et al. in studies of proton transfer in carbonic anhydrase,[52] the same enzyme we investigate in this study. The number of grid points per processor is set to 97 for each dimension. The atomic charges for the solute clusters are determined by the ChelpG scheme[81] in the Gaussian quantum mechanics package[78] at the B3LYP/6-311+G(2d,p) level of theory. The atomic radii are taken from the Amber force field with the exception of Zn(II), which is set to 2.1 Å.[82] The radius for the ion is determined by the first peak of the experimental radial distribution of oxygen atoms in zinc solvated by water.

The continuum calculations are also performed with a polarizable continuum model[83] as implemented in Gaussian 09 using the SMD solvation model.[84] The SMD model is a novel continuum solvation model based on the quantum mechanical charge density of a solute molecule interacting with a continuum description of the surrounding solvent. The UFF (universal force field) radii set[85] is used for all atoms except for Zn(II), which again is given the radius of 2.1 Å. By default, the Gaussian 09 program constructs the solute cavity using the UFF radii, which places a sphere around each solute atom, including hydrogen atoms, using radii scaled by a factor of 1.1. To be consistent with APBS continuum calculations, the dielectric constant for the environment is set to 40.0. The SMD calculation is performed at standard temperature and pressure by default. Optimization is followed by frequency calculation at the level of B3LYP/6-311+G(2d,p). The SMD calculation gives the total free energy of the cluster in aqueous phase, which is the same as computing the free energy change described by the red arrows in Scheme 1. Therefore there is no need to calculate the solvation free energies and gas phase free energies separately. Hence, the deprotonation free energy in the environment is just the difference of the aqueous phase free energies from the SMD calculations. Note that the proton solvation free energy (ΔG_{solv}^{H+}) drops out when calculating the relative pK_a values for wild type and mutated enzymes.

The atomic partial charges of the active site complexes are determined with the AIMALL package,[86] which calculates the atomic charges based on Bader's quantum theory of atoms in molecules technique (QTAIM).[87] The dipole moment (μ) of the active-site water molecule in each complex is estimated by summing up all the atomic dipole moments from the AIMALL calculation. In the atoms in molecules methodology, the molecular dipole moment consists of two components: a fixed charge component, based on the atomic partial charges, and a polarization component. We are using the dipole moment as an indicator of the amount of polarization in the zinc-bound water and hydroxide. The experimental measurements for the dipole moments of water and hydroxide molecules in gas phase are 1.85 D and 1.66 D, respectively.[88] The dipole moments are slightly overestimated by the B3LYP/6-311+G(2d,p) calculation, giving 2.08 D for H_2O and 1.71 D for OH^-.

RESULTS AND DISCUSSION

pK_a of Zinc-Bound Water. As mentioned above, pK_a shifts of the zinc-bound water corresponding to His/Asp mutations were determined experimentally by Kiefer and Fierke.[29] Two CA II variants were examined: H94D and H119D (see Figure 2 for positions of the three histidines at the active site of the native enzyme). In our calculations, we estimate the pK_a change by mutating one histidine at a time for all three histidines at the active site (His94, His96, and His119). The results obtained are summarized in Table 1.

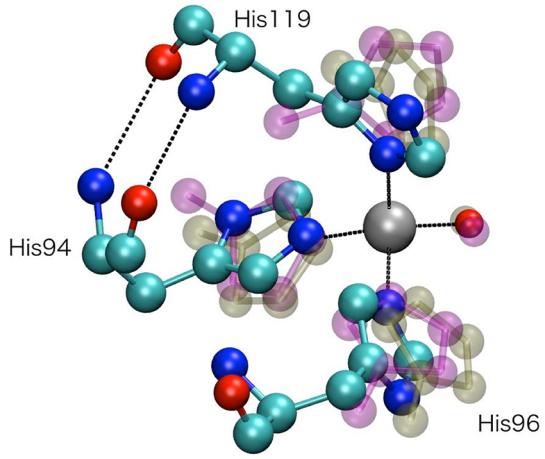

Figure 2. Superposition of cluster structures in the zinc-centered active site of carbonic anhydrase II, including the crystal structure (opaque), optimized protonated structure (transparent, tan), and optimized deprotonated structure (transparent, pink). Hydrogen atoms are hidden for clearer illustration.

Table 1. Free Energy Components of pK_a Calculations for Wild Type and Mutant CA II[a]

CA II	ΔG_{gas}^{deprot}	$\Delta\Delta G_{solv}$	$\Delta\Delta G_{env}^{deprot}$[c]	ΔpK_a	exp
WT	181.93	103.48			
H119D	262.94	25.26	2.79	2.03	1.8[b]
H94D	261.39	27.84	3.82	2.78	2.8[b]
H96D	261.05	29.19	4.83	3.52	

[a]Free energy unit is kcal/mol. [b]Experimental data from ref 29. pK_a values for wild type and variant CA II were estimated by measuring the pH-dependence of the esterase activity of the enzyme. [c]Deprotonation free energy difference between mutant and native enzyme.

The relative shifts in pK_a from experiments based on mutants H94D and H119D are 2.8 and 1.8, with H94D causing a larger change in pK_a. These values are well reproduced by our calculations (2.78 and 2.03). While the change in pK_a for the H96D mutation has not been determined experimentally, the same computational method predicts a shift of 3.52, the largest change of all the mutants. On the basis of the agreement with experiment found for the other mutants, this prediction should be reasonably accurate. Not surprisingly, all His/Asp mutations

dx.doi.org/10.1021/bi201771q | Biochemistry 2012, 51, 5979−5989

of the zinc coordinating ligands do indeed increase the pK_a of zinc-bound water from its value of 6.8 in the wild type enzyme. In other words, the mutations destabilize deprotonation of the zinc-bound water, which in turn impedes CO_2 capture by the enzyme. It is also worth noting that mutations at different positions result in different increases in pK_a, with the order being H96D > H94D > H119D. We will explore the possible reasons causing this functional asymmetry in the following discussion.

As pointed out earlier, the pK_a value is converted from differences in deprotonation free energies in wild type and mutant enzymes based on eq 2. The deprotonation free energy is composed of the free energy change for deprotonation of the active site cluster in gas phase (ΔG_{gas}^{deprot}) and solvation of products and reactants ($\Delta\Delta G_{solv}$) in the deprotonation reaction due to interactions with the environment (listed in Table 1). The deprotonation reaction not only destabilizes the active site cluster in gas phase, but also yields an overall unfavorable solvation of deprotonated versus protonated states. Note that the proton has been omitted from the calculations due to cancellation when calculating free energy differences between wild type and mutant enzymes. Since the solvation free energy of a proton is roughly $\Delta G_{solv}^{H+} = -250$ kcal/mol, the total solvation free energy of a single deprotonation reaction ($\Delta\Delta G_{solv}$) would be favorable for the mutants and the wild type if ΔG_{solv}^{H+} were included. The contribution of proton solvation does not change the overall relative deprotonation free energy between wild type and mutant enzymes tabulated in Table 1. While the gas phase component is comparable to the solvation contribution in the wild type enzyme, the gas phase contribution dominates in deprotonation free energy for all the mutant enzymes due mainly to unfavorable enthalpy changes.

On the basis of the agreement between our calculation and experimental measurements for the pK_a values, we believe the simple continuum model with $\varepsilon = 40$ is sufficient to take into account the simultaneous presence of the remainder of the protein and solvent. To be noted, a paper published recently by Rao et al. compared metal binding affinity to a protein computed with QM/continuum and QM/MM methods.[89] As their calculations show, the solvation contribution estimated with higher dielectric constant in the QM/continuum method tends to yield better agreement with QM/MM methods, which also corroborates the possibility of reproducing experimental data with the ideal choice of dielectric constant.

For comparison, the pK_a shifts are also calculated using the SMD solvation model. The ΔpK_a values estimated with this approach are 5.91, 8.15, and 9.28 for H94D, H119D, and H96D, respectively. While the pK_a shifts are well reproduced by the DFT+APBS method, the SMD polarizable continuum model performs less well. The discrepancy between the two strategies possibly comes from the following: (1) the different treatments of the solvation contribution; (2) the different choices of solute charges and radii; (3) the slightly different cluster structures (the cluster structures taken from gas phase optimization are optimized again in the SMD approach). Challenges in predicting accurate metal−ligand interactions energies using the SMD solvation model, especially in the presence of anionic ligands, have been described elsewhere.[90]

Structural Analysis. The crystal structure of the active site of CA II is shown in Figure 2 together with the optimized protonated and deprotonated clusters. It is worth noting that His119 and His94 form two stabilizing hydrogen bonds with pairs of O−HN interactions in the backbones, whereas His96 sits alone on the opposing side of the active site. Since the cluster model was simplified by truncating the backbones, the hydrogen bonding restraint on His96 no longer exists. Thus the optimized structures of protonated and deprotonated states of the active site for the imidazole models deviate from the original histidine crystal structure slightly, whereas the positions of the imidazole nitrogen atoms that coordinate Zn(II) occupy nearly the same positions. Interestingly, both His94 and His96 are in the same form with the protons on the epsilon nitrogen; however, His119 is in the form with the proton on the delta nitrogen. In other words, the zinc ion coordinates with two epsilon nitrogens (from His94 and His96) and one delta nitrogen (from His 119). This adds to the overall asymmetric structure of the cluster, which in part explains the distinct pK_a shift by His/Asp mutations at different locations (94 or 96 versus 119).

We examine the zinc binding site structure by measuring the distance between the zinc ion and its four ligands (Table 2).

Table 2. Distances between Zn(II) and Its Four Ligands, Including Three Nitrogen Atoms from the Imidazoles and One Water Oxygen Atom for the Crystal Structure and Optimized Protonated and Deprotonated Structures[a]

(Å)	Zn−Nδ_{119}	Zn−Nε_{94}	Zn−Nε_{96}	Zn−O$_w$
crystal	2.11	2.10	2.12	2.05
protonated	2.00	2.00	2.02	2.16
deprotonated	2.07	2.05	2.07	1.88

[a]Numbers are in units of Å.

The optimized structures are in good alignment with the crystal structure (root-mean-square deviation, or rmsd, less than 1.3 Å). As displayed in Figure 2, the tetrahedral structure is fairly well maintained after optimization with ligand-ion-ligand angles all around 110 degrees (measured using the coordinating atoms and the Molden visualization package[91]). The data in Table 2 indicate that the three imidazoles are drawn slightly (less than 5%) toward the zinc ion in both protonated and deprotonated states, with the deprotonated state a little expanded compared to the protonated state. The water and hydroxide ion, however, show opposite behaviors after optimization: the water from the protonated state is pushed out further and the hydroxide from the deprotonated state pulled closer. Hydroxide ion approaches zinc more closely than the water molecule in part because OH^- is less bulky than the water. Additionally, the strong electrostatic attraction between the negative charge on hydroxide and the positively charged zinc ion accounts for the closer interaction. Note that the zinc-bound water in the crystal structure is expected to be in the deprotonated state, which corresponds with the closer approaches of the hydroxide ion compared to imidazole and histidine nitrogens in both crystal and model structures (see Table 2).

In the mutated active sites, the structural changes due to the replacement of one histidine (imidazole) by an aspartate (acetate) are of particular interest because we are studying the effect of mutation on the pK_a change. In principle, acetate may offer two oxygen atoms to coordinate with the zinc ion, thus increasing coordination of zinc from 4- to 5-fold. As seen in Figure 3, however, acetate does not act as a bidentate ligand except for the H94D mutant. Acetate offers only one oxygen atom to the zinc ion in the cases of H96D and H119D. When the acetate is monodentate, the other oxygen atom either hydrogen bonds with the hydrogen atom of water (protonated

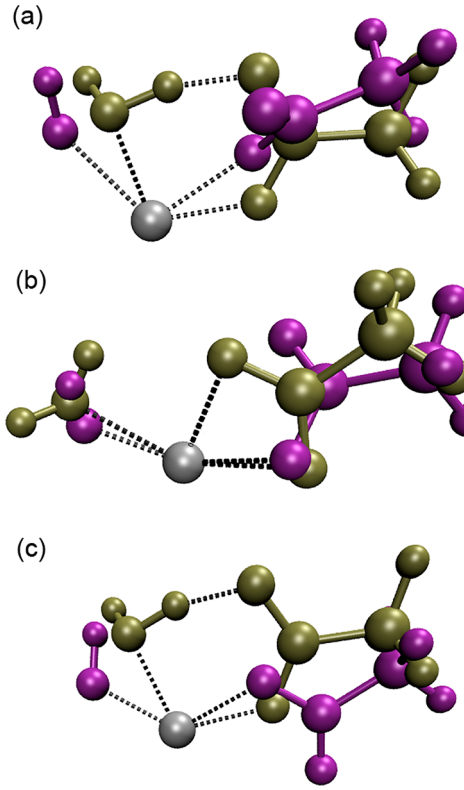

Figure 3. Partial structure of the zinc binding site, including Zn(II) (gray), acetate, and water/hydroxide. The protonated state is represented by tan, and the deprotonated state is represented by pink. Dashed lines connect Zn(II) and coordinating oxygens (see Table 3), and the hydrogen of water to oxygens of acetate within hydrogen bond distance (1.44 Å for H119D, 1.49 Å for H96D). (a) H119D; (b) H94D; (c) H96D.

state) or does not interact with any atom (deprotonated state). The water molecule essentially competes with the Zn(II) for ligation with the acetate molecule.

Coordination of zinc ion is flexible.[98] In bulk water, 6-fold coordination of Zn(II) is reported.[66,82] Although four-coordinate zinc complexes are more commonly seen in zinc proteins,[92] there is strong crystallographic and spectroscopic evidence showing that the binding of certain bidentate ligands to zinc is five-coordinate.[93,94] For example, carboxy-peptidase A (CPA) is a homologue of CA II. At its zinc binding site, the cation is found to be ligated by His69, His196, Glu172, and a water molecule (Figure 4). The Glu172 is bidentate and thus the zinc complex is five-coordinate. Although the detailed catalytic mechanism of carbonic anhydrase still remains unclear, consensus has been reached that the zinc-centered transition state with bicarbonate is five-coordinate.[7,95] Therefore, it is not unexpected that both 4-fold and 5-fold coordination are observed in the CA II aspartic acid mutants. Distances between Zn(II) and its ligands for the mutants are summarized in Table 3.

Similar to the wild type enzyme, the hydroxide anion of the deprotonated state is located closer to zinc than the water molecule of the protonated state in every mutant. Furthermore, imidazole groups expand slightly in the deprotonated states of the mutants, just as they did in the wild type. The distance between Zn(II) and the monodentate acetate (H96D and H119D) is shorter than that between Zn(II) and the bidentate acetate (H94D, protonated). This is likely due to steric effects

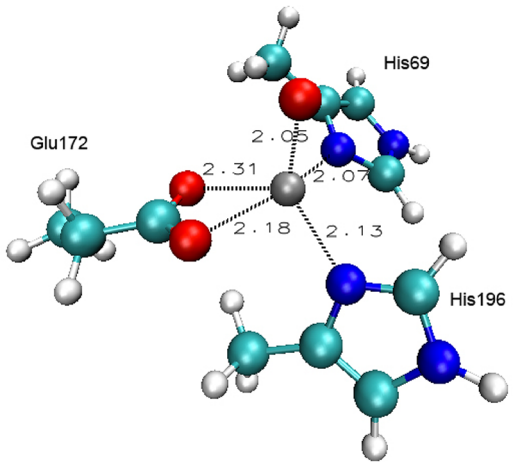

Figure 4. Five-coordinate active site crystal structure of carboxy-peptidase (PDB ID 5CPA). The residues are truncated in the same way as in the CA II system: histidine is represented by imidazole, glutamic acid by acetate. Distances between Zn(II) and its five ligating atoms are labeled (Å).

Table 3. Distances between Zinc Ion and Its Coordinating Ligands Measured from the Mutant Active Site Complex after Optimization (units of Å)[a]

	Zn-119	Zn-94	Zn-96	Zn−O_w
H119D	1.95/3.09	2.02	2.01	2.05
	1.96	2.11	2.13	1.89
H94D	2.02	2.07/2.16	2.04	2.26
	2.12	1.99	2.16	1.87
H96D	2.01	2.01	1.95/3.08	2.05
	2.12	2.08	1.96	1.90

[a]For each mutant, the top row describes the protonated complex and the bottom row, the deprotonated complex. Note that acetate ligands provide only one coordinating oxygen to zinc in H96D and H119D mutants and in the deprotonated state of H94D mutant.

because a bidentate ligand takes up more space in the coordination volume than a monodentate ligand. After deprotonation, the bidentate acetate ligand becomes monodentate (H94D) and contracts to a position closer to Zn(II), while the monodentate acetate ligands (H119D, H96D) stay about the same distance from zinc. All acetate ligands in the deprotonated states approach Zn(II) more closely than the imidazole groups, but not as close as hydroxide. This reflects strong electrostatic interactions between negatively and positively charged ions, and the differences in size between acetate and hydroxide ions.

The molecular structure of the zinc-bound water is also affected by the mutations (Table 4). The average experimental

Table 4. Structural Properties of the Zinc-Bound Water Molecule in Bulk Water and in Wild Type and Mutant CA II[a]

	H−O−H angle	O−H bond1	O−H bond2
BULK	104.5	0.96	0.96
WT	107.0	0.97	0.97
H119D	108.7	1.06	0.96
H94D	106.9	0.97	0.96
H96D	108.7	1.05	0.96

[a]Angles in degrees and bond lengths in Å.

dx.doi.org/10.1021/bi201771q | *Biochemistry* 2012, 51, 5979−5989

Table 5. Charge Distributions Derived from AIMALL for the Active Site Systems of Wild Type and Mutant Enzymes[a]

	Zn	O_w	Wat	His	Asp	μ(Debye)	$\Delta\mu$(Debye)
WT(H_2O)	1.269	−1.148	0.072	0.226		1.915	−0.559
WT(OH^-)	1.251	−1.231	−0.716	0.155		1.356	
119(H_2O)	1.299	−1.199	0.014	0.190	−0.695	1.704	−0.036
119(OH^-)	1.288	−1.231	−0.726	0.117	−0.796	1.669	
94(H_2O)	1.303	−1.135	0.051	0.186	−0.727	2.060	0.605
94(OH^-)	1.284	−1.212	−0.712	0.115	−0.801	2.664	
96(H_2O)	1.296	−1.198	0.018	0.191	−0.701	1.659	0.658
96(OH^-)	1.289	−1.233	−0.733	0.121	−0.733	2.316	

[a]The first column describes the CA II enzyme, the second and third columns give the partial charges on Zn and the oxygen of water/hydroxide. The fourth column (labeled "Wat") is the total charge of the water/hydroxide molecule. The fifth column is the average charge of the imidazole ligands and the sixth column is the charge of the acetate ligand in the mutant complexes. The molecular dipole moment of the zinc-bound water/hydroxide molecule and the dipole change upon deprotonation for each species are also listed in the seventh and eighth columns, respectively (Debye). Charge is in atomic units (a.u.).

H−O−H angle of water in bulk is 104.5° and the O−H bond length is 0.96 Å. In the context of the optimized structure of the zinc-centered active site in wild type CA II, the water structure is slightly expanded, with the bond length stretched by 1% (0.01 Å) and the H−O−H angle increased by 2% (2.5 deg). In the five-coordinate H94D mutant, acetate coordinates zinc as a bidentate ligand and thus does not interact with the water ligand. Consequently the zinc-bound water structure in the H94D mutant closely resembles the wild type. In contrast, hydrogen-bonding between water and acetate in mutants with 4-coordinate ligation of Zn(II) (H96D and H119D) disrupts the structural symmetry of the zinc-bound water. Specifically, the water angle expands another 2 degrees to 108.7°, giving a 4% increase compared to bulk water, and the O−H bond closer to the acetate oxygen atom (bond1) lengthens 10% compared to the other O−H bond. The 0.1-Å extension of a single O−H bond is clearly related to the strong hydrogen-bond interaction with the acetate ligand. These structural changes in zinc-bound water correlate with calculated shifts in the water dipole moment, as described in the next section (see Table 5).

Electrostatics Properties. According to Christianson and Fierke,[96] the pK_a change due to mutations at the active site of the enzyme is a sensitive indicator of changes in the electrostatic environment of Zn(II). Table 5 summarizes the charges of zinc ion and its ligands in wild type and mutant clusters. With substitution of negatively charged aspartate ligands in place of neutral imidazole ligands, the partial charges on zinc and its coordinating ligands shift. Specifically, the partial positive charge on zinc ion is slightly smaller in the wild type than in the mutant cluster by roughly 2.3% in both protonated and deprotonated states. Moreover, the charge of zinc ion shows a mild decrease from the protonated (H_2O) to the deprotonated state (OH^-) by less than 1.6% for all complexes. The partial charge on the oxygen atom of the water molecule is systematically less negative than that of the corresponding hydroxide anion. The molecular charges of the ligands, including water/hydroxide and imidazole, are nearly all lower (either less positive or more negative) in the mutant complexes compared to the wild type complex. This is because the overall charge of the mutant complex is lower than the wild type by 1 unit of charge. This difference of 1 unit charge is distributed over the entire complex, which in turn reduces the charges of all ligands in the mutant complexes. These observations are in reasonable agreement with Bertini's ab initio calculations[97] in which the pK_a of the enzyme is found to be partially determined by electronic properties of the metal complex.

Deprotonation results in different shifts in net molecular charge on the acetate ligand of the mutant complexes, depending on the substitution site. The acetate molecule is more negatively charged in the deprotonated compared to protonated state in all three mutants. The shift of the molecular charge of acetate in the deprotonation reaction shows the following trend: H119D > H94D > H96D. This trend in diminishing change in the acetate charge correlates with the trend in increasing pK_a shift (H119D < H94D < H96D).

Not surprisingly, the dipole moments of the water/hydroxide in the enzyme active site fluctuate around the calculated gas-phase values of 2.08/1.71 D. The variation in dipole moment of water/hydroxide is a result of differences in electronic interactions for each active-site complex, which influence the pK_a shifts. To be more specific, the structure of zinc-bound water in mutant H94D closely resembles the bound water in the wild type complex in terms of angle and bond length. Furthermore, partial charges of the coordinating oxygen for water in the H94D mutant and wild type complex are similar. Consequently, the dipole moment of the zinc-bound water in H94D and wild type are similar, with values slightly smaller than gas phase water (2.06 and 1.92 D, respectively). In contrast, the structure of the zinc-bound water in H96D and H119D mutants is somewhat distorted compared to gas phase water while the partial charges on the coordinating water oxygens are enhanced to more negative values (−1.20 au in mutants vs −1.08 in gas phase). This correlates with smaller water dipole moments in these mutants (1.7 D) compared to gas phase water. In the more crowded five-coordinate protonated mutant, H94D, the zinc-bound water is pushed away from zinc ion by roughly 0.1 Å. On the contrary, the water molecules in both four-coordinate H96D and H119D mutants occupy closer positions to the metal than in the wild type, which presumably relates to the more negative partial charge on the coordinating oxygen atoms of water in these mutants compared to wild type.

The shift in dipole moment of zinc-bound water during deprotonation of water to hydroxide ion is the most relevant property to understanding pK_a shifts. In the wild type enzyme, OH^- is less polarized than H_2O by 0.56 D, which mimics the behavior in the gas phase. In the mutant enzymes, on the contrary, OH^- tends to have a bigger dipole than H_2O except for mutant H119D. In the H119 mutant, the dipole is roughly the same for the zinc-bound water before and after the deprotonation reaction. To summarize, these shifts in dipole moment of zinc-bound water upon deprotonation, $\Delta\mu$, show

the following trend: H119D < H94D < H96D. This ordering pattern agrees exactly with the trend observed earlier in ΔpK_a values (Table 1). This correlation suggests that the dipole moment change in zinc-bound water due to deprotonation is a direct indicator of the pK_a change. In other words, the increase in pK_a with His → Asp mutations applied to specific residues in the carbonic anhydrase II active site may be a consequence of more positive changes in dipole moment in the deprotonation reaction from zinc-bound H_2O to OH^-.

To gain further insight about the catalytic mechanism of carbonic anhydrase, future work will include predicting pK_a shifts due to mutations of active site residues further from the zinc center, investigating the effect of salt concentration and metal substitution on the enzymatic activity, and including dynamical information available from ab initio molecular dynamics simulations. The same computational methodology potentially can be used to study the pK_a shifts in other metalloenzymes as well.

CONCLUSION

Carbonic anhydrase II is one of the most efficient enzymes in nature. CA II converts CO_2 gas into water-soluble bicarbonate ion. The reaction rate is governed by the pK_a of the zinc-bound water in the active site because deprotonation of that water is the rate-limiting step of the catalytic reaction. Experiments have shown that mutation of the direct ligands of zinc, in which one histidine is replaced with a negatively charged aspartic acid, raises the pK_a of that particular water molecule, which in turn impedes the activity of the enzyme. In this study we estimated the pK_a shifts due to mutations at the active site of CA II and investigated changes in structural and electrostatic properties associated with the shifts. We used density functional theory to model the active site as a cluster and a dielectric continuum model to treat the surrounding protein and solvent environment.

The pK_a predictions using this combined approach agreed well with experimental measurements for His/Asp mutations applied to residues 119 and 94. Specifically, these mutations increased the pK_a of zinc-bound water. Prediction of the pK_a shift in the experimentally unmeasured H96D mutant produced this overall asymmetric trend: H119D < H94D < H96D. Decomposition of the free energy difference between mutant and wild type enzymes showed that the increase in pK_a of the mutants is associated with large unfavorable enthalpy changes in gas phase deprotonation reactions.

To gain insight into the source of the pK_a shifts and their asymmetry, we compared the structural properties of wild type and mutant zinc clusters. Histidine ligands in the active site, and the imidazole molecules used to model them, naturally possess asymmetry in terms of the groups that coordinate zinc. H119 coordinates zinc with the delta nitrogen while H94/H96 coordinates with the epsilon nitrogen. Furthermore, mutations of imidazole to aspartate in the active site affect the coordination structure between zinc ion and its ligands, with H94D producing a 5-fold coordination structure around zinc. Mutations at different positions also induce variations in the structure of the zinc-bound water, including the coordination number and lowest energy conformation. These shifts in active site structure help explain why the same type of mutation applied to different residues results in different pK_a changes.

Finally, we carried out an electrostatics analysis to obtain more insights into the pK_a changes due to the mutations. In particular, the partial charges of the oxygen atom of the zinc-bound water/hydroxide and zinc ion were computed based on QTAIM theory. Although the atomic charges do not change by a large amount, the variation in the electrostatic environment due to mutation is significant enough to affect the pK_a of the zinc-bound water. We also found a correlation between the electrostatics, including charges and dipoles of the zinc ligands, and the pK_a shift. On one hand, the change in partial negative charge of the ligating acetate molecule shows trends in diminishing negative charge that follows the trend in increasing shifts in pK_a. On the other hand, the dipole moment change of the zinc-bound water during deprotonation is correlated with the pK_a shift due to mutation. Specifically, increasing shifts in pK_a to less favorable values for deprotonation correspond to enhanced dipole moments of the zinc-bound water upon deprotonation.

AUTHOR INFORMATION

Corresponding Author

*E-mail: slrempe@sandia.gov. Phone: 505-845-0253.

Notes

The authors declare no competing financial interest.

ACKNOWLEDGMENTS

We would like to acknowledge funding from the Sandia Laboratory Directed Research and Development Program and helpful discussions with Dr. Bruce Bunker. Sandia National Laboratories is a multiprogram laboratory operated by Sandia Corporation, a wholly owned subsidiary of Lockheed Martin Corporation, for the U.S. Department of Energy's National Nuclear Security Administration under contract DE-AC04-94AL85000.

REFERENCES

(1) IPCC (2001) The Carbon Cycle and Atmospheric Carbon Dioxide, in *Climate Change 2001: The Scientific Basis*, Cambridge University Press, U.K.

(2) Lindskog, S. (1973) The catalytic mechanism of carbonic anhydrase. *Proc. Natl. Acad. Sci. U.S.A. 70*, 4.

(3) Lindskog, S. (1997) Structure and mechanism of carbonic anhydrase. *Pharmacol. Therapeut. 74*, 1−20.

(4) Jiao, D., and Rempe, S. B. (2011) CO_2 solvation free energy using quasi-chemical theory. *J. Chem. Phys. 134*, 224506−224514.

(5) Hakansson, K., Carlsson, M., Svensson, L. A., and Liljas, A. (1992) Structure of native and apo carbonic anhydrase II and structure of some of its anion-ligand complexes. *J. Mol. Biol. 227*, 1192−1204.

(6) Woolley, P. (1975) Models for metal ion function in carbonic anhydrase. *Nature 258*, 677−682.

(7) Silverman, D. N., and Lindskog, S. (1988) The catalytic mechanism of carbonic anhydrase: implications of a rate-limiting protolysis of water. *Acc. Chem. Res. 21*, 30−36.

(8) Zhang, X., Hubbard, C. D., and van Eldik, R. (1996) Carbonic anhydrase catalysis: A volume profile analysis. *J. Phys. Chem. 100*, 9161−9171.

(9) Kimura, E. (2000) Model studies for molecular recognition of carbonic anhydrase and carboxypeptidase. *Acc. Chem. Res. 34*, 171−179.

(10) Lindskog, S.; Silverman, D. N. (2000) *The Catalytic Mechanism of Mammalian Carbonic Anhydrases*, Birkhauser Verlag, Basel, Switzerland.

(11) Domsic, J. F., Avvaru, B. S., Kim, C. U., Gruner, S. M., Agbandje-McKenna, M., Silverman, D. N., and McKenna, R. (2008) Entrapment of carbon dioxide in the active site of carbonic anhydrase II. *J. Biol. Chem. 283*, 30766−30771.

(12) Liang, J. Y., and Lipscomb, W. N. (1986) Theoretical study of the uncatalyzed hydration of carbon dioxide in the gas phase. *J. Am. Chem. Soc. 108*, 5051−5058.
(13) Merz, K. M., Hoffmann, R., and Dewar, M. J. S. (1989) The mode of action of carbonic anhydrase. *J. Am. Chem. Soc. 111*, 5636−5649.
(14) Jacob, O., Cardenas, R., and Tapia, O. (1990) An ab initio study of transition structures and associated products in $[ZnOHCO_2]^+$, $[ZnHCO_3H_2O]^+$, and $[Zn(NH_3)_3HCO_3]^+$ hypersurfaces. On the role of zinc in the catalytic mechanism of carbonic anhydrase. *J. Am. Chem. Soc. 112*, 8692−8705.
(15) Merz, K. M. (1991) Carbon dioxide binding to human carbonic anhydrase II. *J. Am. Chem. Soc. 113*, 406−411.
(16) Aqvist, J., and Warshel, A. (1992) Computer simulation of the initial proton transfer step in human carbonic anhydrase I. *J. Mol. Biol. 224*, 7−14.
(17) Aqvist, J., Fothergill, M., and Warshel, A. (1993) Computer simulation of the carbon dioxide/bicarbonate interconversion step in human carbonic anhydrase I. *J. Am. Chem. Soc. 115*, 631−635.
(18) Hartsough, D. S., and Merz, K. M., Jr. (1995) Dynamic force field models: Molecular dynamics simulations of human carbonic anhydrase II using a quantum mechanical/molecular mechanical coupled potential. *J. Phys. Chem. 99*, 11266−11275.
(19) Merz, K. M., and Banci, L. (1997) Binding of bicarbonate to human carbonic anhydrase II: A continuum of binding states. *J. Am. Chem. Soc. 119*, 863−871.
(20) Hartmann, M., Merz, K. M., van Eldik, R., and Clark, T. (1998) The important role of active site water in the catalytic mechanism of human carbonic anhydrase II, a semiempirical MO approach to the hydration of CO_2. *J. Mol. Model. 4*, 355−365.
(21) Schutz, C. N., and Warshel, A. (2004) Analyzing free energy relationships for proton translocations in enzymes: carbonic anhydrase revisited. *J. Phys. Chem. B 108*, 2066−2075.
(22) Braun-Sand, S., Strajbl, M., and Warshel, A. (2004) Studies of proton translocations in biological systems: simulating proton transport in carbonic anhydrase by EVB-based models. *Biophys. J. 87*, 2221−2239.
(23) Brauer, M., Perez-Lustres, J. L., Weston, J., and Anders, E. (2002) Quantitative reactivity model for the hydration of carbon dioxide by biomimetic zinc complexes. *Inorg. Chem. 41*, 1454−1463.
(24) Mohammed, O. F., Pines, D., Dreyer, J., Pines, E., and Nibbering, E. T. J. (2005) Sequential proton transfer through water bridges in acid-base reactions. *Science 310*, 83−86.
(25) Domsic, J. F., Williams, W., Fisher, S. Z., Tu, C., Agbandje-McKenna, M., Silverman, D. N., and McKenna, R. (2010) Structural and kinetic study of the extended active site for proton transfer in human carbonic anhydrase II. *Biochemistry 49*, 6394−6399.
(26) Riccardi, D., Konig, P., Prat-Resina, X., Yu, H., Elstner, M., Frauenheim, T., and Cui, Q. (2006) "Proton holes" in long-range proton transfer reactions in solution and enzymes: a theoretical analysis. *J. Am. Chem. Soc. 128*, 16302−16311.
(27) Swanson, J. M. J., Maupin, C. M., Chen, H., Petersen, M. K., Xu, J., Wu, Y., and Voth, G. A. (2007) Proton solvation and transport in aqueous and biomolecular systems: insights from computer simulations. *J. Phys. Chem. B 111*, 4300−4314.
(28) Cui, Q., and Karplus, M. (2003) Is a "proton wire" concerted or stepwise? A model study of proton transfer in carbonic anhydrase. *J. Phys. Chem. B 107*, 1071−1078.
(29) Kiefer, L. L., and Fierke, C. A. (1994) Functional characterization of human carbonic anhydrase II variants with altered zinc binding sites. *Biochemistry 33*, 15233−15240.
(30) March, J. (1985) *Advanced Organic Chemistry*, 3rd ed., John Wiley & Sons Inc, Hoboken, NJ.
(31) Lim, C., Bashford, D., and Karplus, M. (1991) Absolute pK_a calculations with continuum dielectric methods. *J. Phys. Chem. 95*, 5610−5620.
(32) Chipot, C., Pohorille, A. (2007) *Free Energy Calculations. Theory and Applications in Chemistry and Biology*, Springer, New York, NY.
(33) Warshel, A., Sussman, F., and King, G. (1986) Free energy of charges in solvated proteins: microscopic calculations using a reversible charging process. *Biochemistry 25*, 8368−8372.
(34) Warshel, A., and Weiss, R. M. (1980) An empirical valence bond approach for comparing reactions in solutions and in enzymes. *J. Am. Chem. Soc. 102*, 6218−6226.
(35) Sham, Y. Y., Chu, Z. T., and Warshel, A. (1997) Consistent calculations of pK_a's of ionizable residues in proteins: semi-microscopic and microscopic approaches. *J. Phys. Chem. B 101*, 4458−4472.
(36) Sandberg, L., and Edholm, O. (1997) pK_a calculations along a bacteriorhodopsin molecular dynamics trajectory. *Biophys. Chem. 65*, 189−204.
(37) Nielsen, E. J., and McCammon, J. A. (2003) On the evaluation and optimization of protein X-ray structures for pK_a calculations. *Protein Sci. 12*, 14.
(38) Kuhn, B., Kollman, P. A., and Stahl, M. (2004) Prediction of pK_a shifts in proteins using a combination of molecular mechanical and continuum solvent calculations. *J. Comput. Chem. 25*, 1865−1872.
(39) Simonson, T., Carlsson, J., and Case, D. A. (2004) Proton binding to proteins: pK_a calculations with explicit and implicit solvent models. *J. Am. Chem. Soc. 126*, 4167−4180.
(40) Bashford, D., and Karplus, M. (1990) pK_a's of ionizable groups in proteins: atomic detail from a continuum electrostatic model. *Biochemistry 29*, 10219−10225.
(41) Brown, T. N., and Mora-Diez, N. (2006) Computational determination of aqueous pK_a values of protonated benzimidazoles (Part 2). *J. Phys. Chem. B 110*, 20546−20554.
(42) Smiechowski, M. (2009) Theoretical calculation of pK_as of phosphoric (V) acid in the polarisable continuum and cluster-continuum models. *J. Mol. Struct. 924−926*, 170−174.
(43) Leung, K., Nielsen, I. M. B., and Criscenti, L. J. (2009) Elucidating the bimodal acid−base behavior of the water−silica interface from first principles. *J. Am. Chem. Soc. 131*, 18358−18365.
(44) Li, G., and Cui, Q. (2003) pK_a calculations with QM/MM free energy perturbations. *J. Phys. Chem. B 107*, 14521−14528.
(45) Riccardi, D., Schaefer, P., and Cui, Q. (2005) pK_a calculations in solution and proteins with QM/MM free energy perturbation simulations: A quantitative test of QM/MM protocols. *J. Phys. Chem. B 109*, 17715−17733.
(46) Riccardi, D., and Cui, Q. (2007) pK_a analysis for the zinc-bound water in human carbonic anhydrase II: Benchmark for "multiscale" QM/MM simulations and mechanistic implications. *J. Phys. Chem. A 111*, 5703−5711.
(47) Ghosh, N., and Cui, Q. (2008) pK_a of residue 66 in Staphylococcal nuclease. I. Insights from QM/MM simulations with conventional sampling. *J. Phys. Chem. B 112*, 8387−8397.
(48) Ghosh, N., Prat-Resina, X., Gunner, M. R., and Cui, Q. (2009) Microscopic pK_a analysis of Glu286 in cytochrome c oxidase (Rhodobacter sphaeroides): Toward a calibrated molecular model. *Biochemistry 48*, 2468−2485.
(49) Goyal, P., Ghosh, N., Phatak, P., Clemens, M., Gaus, M., Elstner, M., and Cui, Q. (2011) Proton storage site in bacteriorhodopsin: New insights from quantum mechanics/molecular mechanics simulations of microscopic pK_a and infrared spectra. *J. Am. Chem. Soc. 133*, 14981−14997.
(50) Kamerlin, S. C. L., Haranczyk, M., and Warshel, A. (2009) Progress in ab initio QM/MM free-energy simulations of electrostatic energies in proteins: Accelerated QM/MM studies of pK_a, redox reactions and solvation free energies. *J. Phys. Chem. B 113*, 1253−1272.
(51) Bottoni, A., Lanza, C. Z., Miscione, G. P., and Spinelli, D. (2004) New model for a theoretical density functional theory investigation of the mechanism of the carbonic anhydrase: How does the internal bicarbonate rearrangement occur? *J. Am. Chem. Soc. 126*, 1542−1550.
(52) Miscione, G., Stenta, M., Spinelli, D., Anders, E., and Bottoni, A. (2007) New computational evidence for the catalytic mechanism of carbonic anhydrase. *Theoretical Chem. Acc.: Theory, Computat. Modeling (Theoretica Chim. Acta) 118*, 193−201.

(53) Pratt, L. R., and Rempe, S. B. (1999) Quasi-chemical theory and implicit solvent models for simulations. *Simulation and Theory of Electrostatic Interactions in Solution. AIP Conference Proceedings 492*, 30.
(54) Beck, T. L., Paulaitis, M. E., Pratt, L. R. (2006) *The Potential Distribution Theorem and Models of Molecular Solutions*, Cambridge University Press, Cambridge.
(55) Varma, S., and Rempe, S. B. (2007) Tuning ion coordination architectures to enable selective partitioning. *Biophys. J. 93*, 1093–1099.
(56) Varma, S., Sabo, D., and Rempe, S. B. (2008) K^+/Na^+ selectivity in K channels and valinomycin: Over-coordination versus cavity-size constraints. *J. Mol. Biol. 376*, 13–22.
(57) Varma, S., and Rempe, S. B. (2008) Structural transitions in ion coordination driven by changes in competition for ligand binding. *J. Am. Chem. Soc. 130*, 15405–15419.
(58) Rogers, D. M., and Rempe, S. B. (2011) Probing the thermodynamics of competitive ion binding using minimum energy structures. *J. Phys. Chem. B 115*, 14.
(59) Asthagiri, D., Dixit, P. D., Merchant, S., Paulaitis, M. E., Pratt, L. R., Rempe, S. B., and Varma, S. (2010) Ion selectivity from local configurations of ligands in solutions and ion channels. *Chem. Phys. Lett. 485*, 1–7.
(60) Leung, K., Rempe, S. B., and von Lilienfeld, O. A. (2009) Ab initio molecular dynamics calculations of ion hydration free energies. *J. Chem. Phys. 130*, 204507–204511.
(61) Rempe, S. B., Pratt, L. R., Hummer, G., Kress, J. D., Martin, R. L., and Redondo, A. (2000) The hydration number of Li^+ in liquid water. *J. Am. Chem. Soc. 122*, 966–967.
(62) Rempe, S. B., and Pratt, L. R. (2001) The hydration number of Na^+ in liquid water. *Fluid Phase Equilib. 183–184*, 121–132.
(63) Asthagiri, D., Pratt, L. R., and Ashbaugh, H. S. (2003) Absolute hydration free energies of ions, ion–water clusters, and quasichemical theory. *J. Chem. Phys. 119*, 2702–2708.
(64) Rempe, S. B., Asthagiri, D., and Pratt, L. R. (2004) Inner shell definition and absolute hydration free energy of $K^+(aq)$ on the basis of quasi-chemical theory and ab initio molecular dynamics. *Phys. Chem. Chem. Phys. 6*, 1966–1969.
(65) Hummer, G., Pratt, L. R., and García, A. E. (1996) Free energy of ionic hydration. *J. Phys. Chem. 100*, 1206–1215.
(66) Asthagiri, D., Pratt, L. R., Paulaitis, M. E., and Rempe, S. B. (2004) Hydration structure and free energy of biomolecularly specific aqueous dications, including Zn^{2+} and first transition row metals. *J. Am. Chem. Soc. 126*, 1285–1289.
(67) Jiao, D., Leung, K., Rempe, S. B., and Nenoff, T. M. (2010) First principles calculations of atomic nickel redox potentials and dimerization free energies: A study of metal nanoparticle growth. *J. Chem. Theory Comput. 7*, 485–495.
(68) LaViolette, R. A., Copeland, K. L., and Pratt, L. R. (2003) Cages of water coordinating Kr in aqueous solution. *J. Phys. Chem. A 107*, 11267–11270.
(69) Ashbaugh, H. S., Asthagiri, D., Pratt, L. R., and Rempe, S. B. (2003) Hydration of krypton and consideration of clathrate models of hydrophobic effects from the perspective of quasi-chemical theory. *Biophys. Chem. 105*, 323–338.
(70) Sabo, D., Rempe, S. B., Greathouse, J. A., and Martin, M. G. (2006) Molecular studies of the structural properties of hydrogen gas in bulk water. *Mol. Simul. 32*, 269–278.
(71) Sabo, D., Varma, S., Martin, M. G., and Rempe, S. B. (2007) Studies of the thermodynamic properties of hydrogen gas in bulk water. *J. Phys. Chem. B 112*, 867–876.
(72) Asthagiri, D., Merchant, S., and Pratt, L. R. (2008) Role of attractive methane-water interactions in the potential of mean force between methane molecules in water. *J. Chem. Phys. 128*, 244512–244517.
(73) Varma, S., Rogers, D. M., Pratt, L. R., and Rempe, S. B. (2011) Design principles for K^+ selectivity in membrane transport. *J. Gen. Physiol. 137*, 479–488.
(74) Warshel, A. (1981) Calculations of enzymatic reactions: calculations of pK_a, proton transfer reactions, and general acid catalysis reactions in enzymes. *Biochemistry 20*, 3167–3177.
(75) Rogers, D. M., Jiao, D., Pratt, L. R., and Rempe, S. B. (2012) Structural models and molecular thermodynamics of hydration of ions and small molecules. *Annu. Rep. Computat. Chem. (In print)*, 7–14.
(76) Grabowski, P., Riccardi, D., Gomez, M. A., Asthagiri, D., and Pratt, L. R. (2002) Quasi-chemical theory and the standard free energy of $H^+(aq)$. *J. Phys. Chem. A 106*, 9145–9148.
(77) DeLano, W. L. (2011) *The PyMOL Molecular Graphics System*, 1.3 ed., Schrodinger LLC, San Carlos, CA.
(78) Frisch, M. J. T., G. W.; Schlegel, H. B.; Scuseria, G. E.; Robb, M. A.; Cheeseman, J. R.; Scalmani, G.; Barone, V.; Mennucci, B.; Petersson, G. A.; Nakatsuji, H.; Caricato, M.; Li, X.; Hratchian, H. P.; Izmaylov, A. F.; Bloino, J.; Zheng, G.; Sonnenberg, J. L.; Hada, M.; Ehara, M.; Toyota, K.; Fukuda, R.; Hasegawa, J.; Ishida, M.; Nakajima, T.; Honda, Y.; Kitao, O.; Nakai, H.; Vreven, T.; Montgomery, Jr., J. A.; Peralta, J. E.; Ogliaro, F.; Bearpark, M.; Heyd, J. J.; Brothers, E.; Kudin, K. N.; Staroverov, V. N.; Kobayashi, R.; Normand, J.; Raghavachari, K.; Rendell, A.; Burant, J. C.; Iyengar, S. S.; Tomasi, J.; Cossi, M.; Rega, N.; Millam, N. J.; Klene, M.; Knox, J. E.; Cross, J. B.; Bakken, V.; Adamo, C.; Jaramillo, J.; Gomperts, R.; Stratmann, R. E.; Yazyev, O.; Austin, A. J.; Cammi, R.; Pomelli, C.; Ochterski, J. W.; Martin, R. L.; Morokuma, K.; Zakrzewski, V. G.; Voth, G. A.; Salvador, P.; Dannenberg, J. J.; Dapprich, S.; Daniels, A. D.; Farkas, Ö.; Foresman, J. B.; Ortiz, J. V.; Cioslowski, J.; Fox, D. J. (2009) *Gaussian 09, Revision A.1*, Gaussian, Inc., Wallingford, CT.
(79) Baker, N. A., Sept, D., Joseph, S., Holst, M. J., and McCammon, J. A. (2001) Electrostatics of nanosystems: Application to microtubules and the ribosome. *Proc. Natl. Acad. Sci. 98*, 10037–10041.
(80) Warshel, A., Naray-Szabo, G., Sussman, F., and Hwang, J. K. (1989) How do serine proteases really work? *Biochemistry 28*, 3629–3637.
(81) Breneman, C. M., and Wiberg, K. B. (1990) Determining atom-centered monopoles from molecular electrostatic potentials. The need for high sampling density in formamide conformational analysis. *J. Comput. Chem. 11*, 361–373.
(82) Ohtaki, H., and Radnai, T. (1993) Structure and dynamics of hydrated ions. *Chem. Rev. 93*, 1157–1204.
(83) Cossi, M., Barone, V., Cammi, R., and Tomasi, J. (1996) Ab initio study of solvated molecules: a new implementation of the polarizable continuum model. *Chem. Phys. Lett. 255*, 327–335.
(84) Marenich, A. V., Cramer, C. J., and Truhlar, D. G. (2009) Universal solvation model based on solute electron density and on a continuum model of the solvent defined by the bulk dielectric constant and atomic surface tensions. *J. Phys. Chem. B 113*, 6378–6396.
(85) Rappe, A. K., Casewit, C. J., Colwell, K. S., Goddard, W. A., and Skiff, W. M. (1992) UFF, a full periodic table force field for molecular mechanics and molecular dynamics simulations. *J. Am. Chem. Soc. 114*, 10024–10035.
(86) Keith, T. A. (2011) *AIMALL*, TK Gristmill Software, Overland Park, KS.
(87) Bader, R. F. W. (1991) A quantum theory of molecular structure and its applications. *Chem. Rev. 91*, 893–928.
(88) Nelson, R. D. J., Lide, D. R. J., Maryott, A. A. (1967) Selected values of electric dipole moments for molecules in the gas phase, National Bureau of Standards, Washington, DC.
(89) Rao, L., Cui, Q., and Xu, X. (2010) Electronic properties and desolvation penalties of metal ions plus protein electrostatics dictate the metal binding affinity and selectivity in the copper efflux regulator. *J. Am. Chem. Soc. 132*, 18092–18102.
(90) Gutten, O., Besseova, I., and Rulisek, L. (2011) Interaction of metal ions with biomolecular ligands: how accurate are calculated free energies associated with metal ion complexation? *J. Phys. Chem. A 115*, 11394–11402.
(91) Schaftenaar, G., and Noordik, J. H. (2000) Molden: a pre- and post-processing program for molecular and electronic structures. *J. Comput.-Aided Mol. Des. 14*, 12.

(92) Ryde, U. (1996) The coordination of the catalytic zinc ion in alcohol dehydrogenase studied by combined quantum-chemical and molecular mechanics calculations. *J. Comput.-Aided Mol. Des. 10*, 153−164.
(93) Boiwe, T., and Branden, C.-I. (1977) X-ray investigation of the binding of 1,10-phenanthroline and imidazole to horse-liver alcohol dehydrogenase. *Eur. J. Biochem. 77*, 173−179.
(94) Sartorius, C., Dunn, M. F., and Zeppezauer, M. (1988) The binding of 1,10-phenanthroline to specifically active-site cobalt(II)-substituted horse-liver alcohol dehydrogenase. *Eur. J. Biochem. 177*, 493−499.
(95) Berg, J. M., Tymoczko, J. L., Stryer, L. (2002) *Biochemistry*, 5th ed., W H Freeman, New York, NY.
(96) Christianson, D. W., Fierke, C. A. (1996) ChemInform Abstract: Carbonic anhydrase: evolution of the zinc binding site by nature and by design, *ChemInform 27*.
(97) Bertini, I., Luchinat, C., Rosi, M., Sgamellotti, A., and Tarantelli, F. (1990) pK_a of zinc-bound water and nucleophilicity of hydroxo-containing species. Ab initio calculations on models for zinc enzymes. *Inorg. Chem. 29*, 1460−1463.
(98) Dokmanic, I., Sikic, M., and Tomic, S. (2008) Metals in proteins: correlation between the metal-ion type, coordination number and the amino-acid residues involved in the coordination. *Acta. Cryst. D64*, 257−263.